Food Research International 222 (2025) 117766

Contents lists available at ScienceDirect

Food Research International

journal homepage: www.elsevier.com/locate/foodres

Tristearin and C12–18 saturated fatty acids blends: Interplay between eutectic phase behaviour and polymorphic transition

Serena Bertoni [a,*], Elena Simone [b], Beatrice Albertini [a], Nadia Passerini [a]

[a] Department of Pharmacy and Biotechnology, University of Bologna, Via S. Donato 19/2, 40127 Bologna, Italy
[b] Department of Applied Science and Technology, Politecnico di Torino, Torino 10129, Italy

ARTICLE INFO

Keywords:
SAXS
Polymorphism
Triacylglycerols
Fat blends
Minor components

ABSTRACT

This study explores the impact of free fatty acids (FAs) with varying chain lengths (C12-C18) on the crystallization behaviour, crystal structure and polymorphic stability of tristearin (SSS), a long-chain saturated triacylglycerol (TAG). SSS-based blends containing different FAs were crystallized into spherical microparticles, and their solid-state organization was investigated using polarized light microscopy, differential scanning calorimetry, and high-resolution synchrotron small and wide-angle X-ray scattering. We found that the α-polymorph of SSS is miscible with up to 10 wt% of chain-length-matched FAs (C18), forming a solid solution characterized by a single lamellar phase with *d*-spacing similar to pure α-SSS. As the chain length mismatch increases (C12 > C14 > C16), miscibility with SSS decreased. Time-resolved SAXS revealed a direct correlation between the degree of SSS/FA miscibility and the kinetics of the α-to-β polymorphic transition in SSS. Lauric acid (LA, C12) exhibited immiscible monotectic behaviour with β-SSS and only partially miscible eutectic behaviour with α-SSS, with LA solubility limit in α-SSS between 2.5 and 5 %. In α-SSS/LA blends, aging led to reduced α-SSS crystallite size and a progressive increase in the thickness of the FA-rich phase, while *d*-spacing remains unchanged. The accelerated α → β polymorphic conversion is attributed to a possible interplay of factors: thermodynamic changes in SSS polymorph stability due to partial miscibility with the FA as well as factors arising from eutectic phase behaviour: reduced crystallite size (microstructural effect) and lattice defects introduced by LA incorporation (molecular-level effect). Overall, this work provides the first experimental evidence linking the eutectic phase behaviour of solid TAG-based mixtures with the kinetic of polymorphic transitions, offering new insights into the structural dynamics and long-term stability of complex fat systems.

1. Introduction

Triacylglycerols (TAGs) are the primary components of solid edible fats and represent the structural base of many lipid-based materials with applications in the food, cosmetic, and pharmaceutical industries. They can crystallize in three main polymorphic forms, α, β', and β, each exhibiting distinct molecular packing, physical properties, and stability (Sato, 2018). In addition, the physical properties of TAGs are influenced by their mixing behaviour with other lipids, the so-called "minor components", such as partial glycerides, phospholipids or fatty acids. In fact, most natural and industrially produced edible fats are mixtures of different TAGs plus other lipidic molecules (Metin & Hartel, 2005).

One of the most efficient and cost-effective strategies to modify the crystallization and structural features of pure TAGs is through physical blending with specific minor components that act as additives. Over the years, extensive research has explored the role of minor components in fat crystallization (Ribeiro et al., 2015). The studies conducted so far have primarily focused on their influence on the crystallization kinetic, particularly regarding nucleation and crystal growth. Depending on the specific composition and interaction of the mixture, minor components can either hinder nucleation (if they disrupt crystal nucleus formation) or impede crystal growth (if they hinder the attachment of TAG molecules at the already formed nuclei); otherwise, nucleation can be promoted if minor components act as templates (Yang et al., 2024). Other research investigated the mixing phase behaviour of TAG-based systems containing minor components, focusing on the development of phase diagrams to understand the solid–liquid transitions of these systems. A recurring observation across these studies is the importance of structural similarity between TAG molecules and the additives in determining the phase behaviour of the mixture. Specifically, three main types of mixing

* Corresponding author.
E-mail address: serena.bertoni4@unibo.it (S. Bertoni).

https://doi.org/10.1016/j.foodres.2025.117766
Received 29 July 2025; Received in revised form 22 September 2025; Accepted 25 October 2025
Available online 30 October 2025

behaviour were identified: (i) miscible components in the solid phase, forming a continuous solid solution; (ii) immiscible components with eutectic behaviour (showing a melting temperature depression for both species) or with monotectic behaviour (only one component suffers the melting temperature depression); and (iii) molecular compound formation, where the two components interact at the molecular level to create a stoichiometric crystalline compound with a well-defined composition and structure (Macridachis-González et al., 2020).

Although the phase behaviour of TAG-based systems containing minor components has been relatively well investigated, the structural implications of their addition remain poorly understood. While structural similarity is often considered a prerequisite for inclusion into TAG crystals as solid solutions, little is known about how these additives affect structural organization across different length scales, such as lamellar packing, crystallite morphology, and bulk microstructure. These features are not only related to morphology and functional properties of the resulting blend, but also play a critical role in determining the thermodynamic and kinetic stability of the system. Over time, and under varying temperature and humidity conditions, TAG-based blends might undergo complex phase transitions that can lead to changes in texture, appearance, and mouth-feel, directly affecting food quality and shelf life, as well as release properties of incorporated active agents. For instance, in chocolate, the transformation of cocoa butter from polymorph V to the more stable polymorph VI is linked to fat bloom, a whitish surface defect that negatively impacts consumer perception (Loisel et al., 1998). Certain selected additives retarded fat blooming and stabilized the polymorph V of cocoa butter, which has the desirable melting profile, appearance, and mouth sensation. The use of additives to control cocoa butter polymorphism is probably the application that has been investigated the most (Garti et al., 1986; K. W. Smith et al., 2011; Tietz & Hartel, 2000). Similarly, improper control of lipid polymorphism can lead to variable and altered release behaviour of bioactive compounds encapsulated in lipid-based formulations (Bertoni et al., 2024; Dos Santos Carvalho et al., 2021; Pluntze et al., 2023). Therefore, monitoring phase transitions and stabilizing the desired crystal forms are essential for maintaining product functionality and ensuring consistent properties throughout storage. As a matter of fact, most studies about TAG-based blends overlook polymorphic transitions occurring during storage, despite their significant impact on long-term stability and performance. As a result, no general rules currently exist to predict how a given additive will affect TAG crystallization, polymorphic behaviour and solid state stability. This lack of structural insight limits our ability to assess or design stable multicomponent lipid systems, especially with regard to their susceptibility to crystal defects, phase transitions and structural reorganization over time.

Among the various minor components, polar lipids such as monoacylglycerols (MAGs) (Liu et al., 2021, Liu et al., 2022), sucrose esters (Puppo et al., 2006; Tangsanthatkun & Sonwai, 2019) and phospholipids (P. R. Smith, 2000; Ye et al., 2023) are the most studied, while free fatty acids (FAs) remain relatively underexplored, despite being naturally present in nearly all edible fats. Even-numbered fatty acids are known to crystallize in at least seven crystalline forms, A_2, A_{super}, B_o, B_m, E_o, E_m, and C (Moreno et al., 2007). The few available studies suggest that FAs can significantly impact the crystal structure and material properties of natural fats and pure TAGs. For example, lauric, palmitic, and oleic acids (at concentrations of 2.5–5 %) were found to delay the crystallization of purified coconut oil at 15 °C (Gordon & Rahman, 1991). A similar trend was observed upon the addition of 15 % lauric acid and the inhibition of crystallization was related to the molecular dissimilarity between coconut oil and the additives (Chaleepa et al., 2010). In contrast, lauric acid accelerated the crystallization rate of trilaurin (P. R. Smith et al., 1994). In chocolate, stearic acid did not significantly alter the early crystallization of saturated TAGs but slowed down the subsequent crystallization of other cocoa butter TAGs, mainly corresponded to the monounsaturated TAGs (Loisel et al., 1998). These findings indicate that the available studies have yielded inconsistent and occasionally conflicting results.

To address these gaps, this study investigates the effect of saturated free fatty acids (FAs) with chain lengths ranging from C12 to C18 on the crystallization, polymorphic behaviour, and solid-state stability of a tristearin (SSS). SSS is a major component of various animal and plant-based fats, particularly hard fats like cocoa butter, tallow, and shea butter (Denke & Grundy, 1991; Gunstone, 2004). Rather than using a natural fat mixture, SSS was selected as model lipid because saturated monoacid TAGs exhibit simple and well-characterized monotropic polymorphism. This makes it a suitable and rational model system for studying fat crystallization and polymorphic transitions in a controlled and reproducible manner, in contrast to the complexity of natural TAG blends compared to more complex TAG mixtures (Oh et al., 2005; Silva et al., 2014; Simone et al., 2024; Da Silva et al., 2016). High resolution time-resolved synchrotron small-angle (SAXS) analyses is used to investigate the structural organization and transformation pathways of binary systems of SSS and different FAs. The combination of SAXS data with DSC, PLM and wide-angle X-ray scattering (WAXS) enables to provide detailed insights into the blends structure at the nano- and micro-length scales. Particular emphasis is placed on evaluating their mutual miscibility in the solid state as well as on the nano/microstructures (e.g. size of the crystalline domains), with the aim of identifying the link between phase behaviour, structural properties and polymorphic transition of the TAG.

2. Materials and methods

2.1. Materials

Tristearin (SSS, Dynasan®118, purity >99 %) was kindly supplied by IOI Oleo. Stearic acid (SA, purity ≥95 %), palmitic acid (PA, purity ≥95 %), myristic acid (MA, purity ≥95 %) and lauric acid (LA, purity 99 %) were purchased from Merck.

2.2. Methods

2.2.1. Preparation of the SSS-based binary mixtures

Binary mixtures consisting in SSS and FAs were crystallized in form of spherical microspheres by spray-congealing technology (Albertini et al., 2008; Bertoni et al., 2018). This technology allowed the formation of solid microspheres by atomization of a molten mixture, followed by crystallization in the cooling chamber kept at room temperature (25 °C). Briefly, the components (SSS and FA at specific mass % ratios) were weighted, blended as powders melted at 90 °C and homogenized for several minutes using a magnetic stirring. The process parameters include the temperature of the nozzle and the inlet air pressure, which were set at 70 °C and 2 bar, respectively. After crystallization in the cooling chamber, the samples were kept at 25 °C/60 % R.H. The blends names and compositions are reported in Table 1.

2.2.2. Differential scanning calorimetry

Differential scanning calorimetry (DSC) was performed with a DSC-6 PerkinElmer apparatus (Perkin Elmer, Beaconsfield, UK). The samples (4–6 mg average mass) were accurately weighed into aluminum pans.

Table 1
Composition of the SSS/FA_S blends.

Blends	Composition % *w/w*				
	SSS	LA	MA	PA	SA
90SSS/10LA	90	10			
90SSS/10MA	90		10		
90SSS/10PA	90			10	
90SSS/10SA	90				10
95SSS/5LA	95	5			
97.5SSS/2.5LA	97.5	2.5			

The DSC scans consisted in heating ramps from 25 to 90 °C with scanning rate of 2 °C/min under a nitrogen flow of 10 mL/min. To allow equilibration of the samples, 5 min isotherms at the starting temperatures were applied before each scan. The onset melting temperatures (T_{onset}) were taken at the intersection of the baseline with the tangent to the left side of the peaks of the heating scans and enthalpy values (J/g) were determined by integrating the DSC peaks of the heating scans. DSC measures were performed at various timepoints (1, 2, 7, 14, 30 and 90 days) during storage.

2.2.3. Powder X-ray diffraction (PXRD)

X-ray powder diffraction analysis were performed using an X'Pert powder diffractometer (Malvern Panalytical, Almelo, NL, USA) equipped with a graphite monochromator in the diffracted beam. Cu Kα radiation was used (40 mA, 40 kV) and the wavelength was 0.154 nm. The spectra were obtained in the range 3°–30° 2θ.

2.2.4. Synchrotron small and wide angle x-ray scattering (SAXS/WAXS)

Small Angle X-ray Scattering (SAXS) analysis were performed at the Austrian SAXS beamline of the Elettra Synchrotron (Trieste, Italy). The incident beam energy was set at 8 keV (λ = 0.154 nm). The SAXS range was set from a q-value of 0.1 to ca. 7 nm^{-1}. The SAXS detector was a Pilatus3 1 M, and, in case of simultaneous SAXS/WAXS measurements, and a Pilatus3 1 M and A Pilatus 100 k detector were used.

Microspheres were loaded into glass capillaries of 1.5 mm outer diameter (Hilgenberg, Maisfeld, Germany) and subjected to:

- static measurements at 25 °C with an exposure time of 20 s;
- 4-steps thermal profile consisting in: heating ramp from 25 to 90 °C at 10 °C/min; isothermal step at 90 °C for 5 min; cooling ramp from 90 to 30 °C at 10 °C/min and two isothermal steps, the first at 30 °C for 60 min, followed by the second at 40 °C for additional 60 min. Data were collected with an exposure period of 20 s and an exposure time of 60 s.

Data analysis was carried out with OriginPro2022 (OriginLab, Massachusetts). The Bragg peaks (first, second and third order) corresponding to the different lamellar structures were identified in the SAXS patterns. Each peak was individually processed by applying a baseline correction and then fitted using Voigt type functions. The peaks maxima (q values) were plotted against their corresponding order of diffraction and linearly interpolated. The characteristics lamellar d-spacing (Å) was obtained using the slope of the fitted line in the formula:

$$d = \frac{2\pi}{q} \quad (1)$$

2.2.5. Crystalline domain size

The average size (D, in nm) of the crystallites was estimated based on the first-order SAXS peak using the Scherrer equation, which relates the diffraction peak broadening to the size of sub-micrometer crystallites (Acevedo et al., 2012):

$$D = \frac{K\lambda}{FWHM(2\theta)\cos\theta} \quad (2)$$

where, FWHM (full width at half maximum) is the width in radians of the diffraction maximum measured at half-height between the background and the peak, θ is the diffraction angle and λ is the wavelength of the X-rays. K (Scherrer constant) is a dimensionless number determined by the crystallite shape; in the absence of detailed shape information, K = 0.9 is a good approximation. The values of FWHM were calculated by fitting the raw data by a Voigt function.

2.2.6. Kinetic of polymorphic transition

For the construction of the kinetic curves of the SSS polymorphic transition during the isothermal phase at 40 °C, the first order SAXS peaks were analysed using a Python script to automatically perform peak fitting at each time point. For each curve, following a baseline correction, the peaks were fitted with Lorentzian and Voigt functions through constrained least-squares regression, and the model providing the best fit was selected; in all cases, the Voigt profile consistently yielded the best results. The ratio of the two polymorphs (α-SSS and β-SSS) was determined by dividing the area of each peak by the sum of both peak areas.

2.2.7. Polarized optical microscopy

Microscopy experiments were performed using a Nikon Eclipse E400 polarizing optical microscope equipped with a Mettler-Toledo (Novate Milanese, Italy) hot stage apparatus and a Nikon Digital Net Camera DN100 camera for image acquisition. For sample preparation, about 5 mg of microspheres were placed onto a glass slide, heated to 70 °C and held for 5 min in order to obtain an isotropic melt, then covered with a coverslip, resulting in a thin film of sample and finally cooled to room temperature. The application of a polarizer allowed to identify the solid phase as it appears brightly coloured due to birefringence. The slides containing the thin layers were imaged immediately after crystallization and after 30 days of aging.

3. Results and discussion

3.1. Characterization of the pure components

The polymorphism of SSS, as other monoacid saturated TAGs, is well known. SSS molecules stack side by side into a double-chain length (2 L) layers called lamellae, while from the top view different subcell structures can be identified, giving three main polymorphic forms: α, β', and β, which are monotropically related. Commercial SSS is available in the stable β-form, while upon crystallization from the melt, α-SSS is obtained. The characteristic short (SAXS) and long spacing (PXRD) patterns of the two forms are shown in Fig. 1SI. The d-spacing values, corresponding to the lamellar thickness, were 50.5 Å and 44.8 Å for α-SSS and β-SSS, respectively, consistently with literature values (Bertoni et al., 2024; Van Langevelde et al., 2001).

The normal chain monocarboxylic acids with even number of carbon atoms were known to exist in at least seven crystalline forms which are called A_2, A_{super}, B_o, B_m, E_o, E_m and C. Pure FAs (LA, MA, PA, and SA) showed one melting endotherm upon heating. Experimental melting temperatures (T_{onset}) and enthalpy (kJ/mol) values are reported in Table 2. Melting peak temperatures values were consistent with the monoclinic C form, which is the most stable phase at room temperature (Moreno et al., 2007; Seilert et al., 2021). This was further confirmed by PXRD analysis (Fig. 2SI). The powder patterns of all raw FAs corresponded to the calculated patterns obtained from single crystal analysis of the polymorph C, using data from the Cambridge Crystallographic Data Centre (CCDC). The refcodes for these data sets are LAURAC05

Table 2
Parameters of pure FAs (polymorph C). Melting temperatures and enthalpies measured by DSC analysis; experimental short and long spacing values; theoretical d-spacing for C polymorph calculated basing on Eq. 3.

FA	Melting temperature (°C)	Enthalpy of fusion (kJ/mol)	Short spacing values from PXRD (Å)	Long spacing values from SAXS (Å)	Long spacing values calculated from unit cell parameters (Å)
LA	44.2 ± 0.5	34.92 ± 1.50	0.371; 0.411	27.3	27.41
MA	53.2 ± 1.4	46.29 ± 1.29	0.369; 0.412	31.5	31.53
PA	60.5 ± 1.0	52.25 ± 1.61	0.370; 0.413	35.7	35.67
SA	70.8 ± 0.6	59.55 ± 1.80	0.369; 0.413	39.8	39.84

(CCDC 738617), ZZZOEG03 (CCDC 738618), YEFWEM01 (CCDC 738619) and STARAC06 (CCDC 1263284). In the small-angle region (Fig. 3SI), the series of equally distanced Bragg peaks indicate that FAs possess a lamellar structure and the interplanar distances (*d*-spacing values) increased with the chain length (Table 2). In the SAXS patterns, additional small-intensity peaks were detected at low *q* values, which represent the first order peaks of TAGs analogues with longer chains (e.g. C20 for SA) as impurities. The experimental *d*-spacing values calculated from SAXS patterns for each FAs were finally compared with the theoretical values calculated basing on unit cell parameters of polymorph C (refcodes reported above) using Eq. 3:

$$d\ spacing = c^{*} \text{sen}\ \beta \quad (3)$$

where c is the unit cell parameter in the z-direction, and β is the tilting angle of the hydrocarbon chains toward the plane of the methyl end groups (Hernández-Veloz et al., 2023). The values of c and β were obtained from unit cell parameters reported by Moreno et al. (Moreno et al., 2007).

3.2. SSS blends with 10 % of FAs

3.2.1. Polymorphism and thermal properties

DSC analysis of SSS-based mixtures with 10 % *w*/w of FAs at various times of stabilization/aging at 25 °C are displayed in Fig. 1.

The heating thermograms of 90SSS/10LA and 90SSS/10MA systems analysed right after crystallization showed four thermal events: a low-temperature endothermic peak (at 41 °C and 48 °C for LA and MA systems, respectively), the melting peak of α-SSS at about 50 °C immediately followed by its recrystallization (i.e. the exothermic peak) in the stable β-form, and finally the melting of β-SSS. As expected, the melting

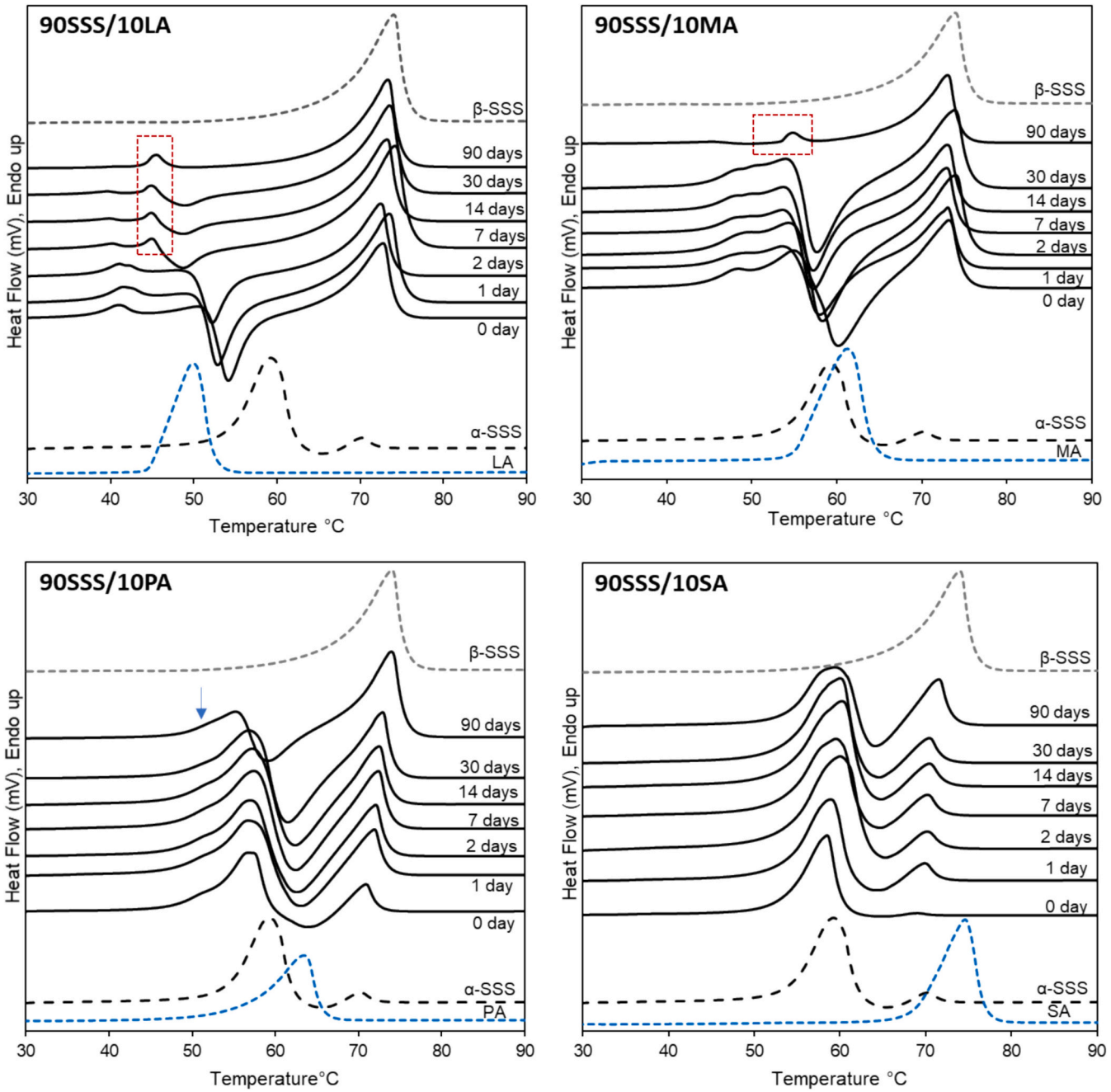

Fig. 1. DSC curves of SSS/FAs samples at various times after crystallization compared to α-SSS and pure FAs.

peak of α-SSS in the blends have a depressed temperatures whereas the melting of the β-SSS in the blends can be observed above 70 °C at a similar temperature to that detected for pure SSS.

The low-melting peak at 41 °C (T_{Onset} = 39 °C) and 48 °C (T_{Onset} = 46 °C) observed in freshly crystallized samples containing LA and MA, respectively, could be attributed either to an eutectic melting or to a lower-melting metastable polymorph of the fatty acids. These hypotheses will be discussed in the following paragraphs. During storage, this low-temperature peak evolved from a single to a double event, as evident in 90SSS/10LA system aged for 2 days and in 90SSS/10MA system aged 7–30 days. Interestingly, the DSC curved showed a change after 7 days (in case of LA-containing systems) or 90 days (in case of MA-containing systems): the two low-temperature peaks disappeared and were replaced by a new single sharp peak at 46 °C (T_{Onset} = 44 °C) and 55 °C (T_{Onset} = 54 °C) for LA and MA-containing samples, respectively, evidenced in red boxes. Considering the peak temperatures and enthalpies, it is reasonable to attribute these peaks to the C polymorphs of LA and MA (Moreno et al., 2007). This phase change coincided with the disappearance of the signals related to the α-SSS, indicating its complete conversion to the β stable form. The data suggest that, in SSS/FA blends with a 90/10 composition, used as a representative TAG-minor component system, C12 and C14 FAs are immiscible with β-SSS, coexisting as separate phases during aging.

In contrast, the DSC curves of 90SSS/10PA and 90SSS/10SA indicated that SSS remained in the α-form up to 90 days. For PA-containing systems, it can be noted an additional low-temperature peak visible as a shoulder of the α-SSS melting peak with low enthalpy (blue arrow). In addition, a consideration should be made regarding the attainment of equilibrium. True thermodynamic equilibrium is assumed to occur only when SSS fully converts to the β form; however, such solid-state conversions are typically slow, often requiring months, because the α form is kinetically stabilized. Based on our observations, equilibrium appears to have been reached for SSS/LA and SSS/MA, but not for SSS/PA and SSS/SA blends. Moreover, the DSC data do not enable accurate quantification of the amount of SSS that has undergone transformation from the α-form to the β-form. Therefore, SAXS analysis was performed on 90SSS/10FAs samples aged for 30 days and their patterns are reported in Fig. 2. The small-angle peaks originate from the lamellar periodicity of the fat crystals, reflecting the regular stacking of acyl chains and terminal groups along the lamellar structure. The position of these peaks was used to calculate the lamellar *d*-spacing, providing a quantitative measure of the layers. The *d*-spacing of the multiple phases observed in the binary mixtures are reported in Table 3. Regarding the polymorphic occurrence of SSS, SAXS patterns confirmed the DSC data: the mixture 90SSS/10LA

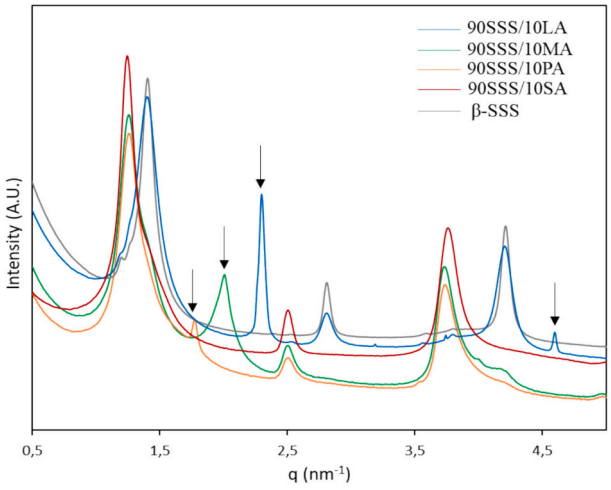

Fig. 2. SAXS patterns of 90SSS/10FAs systems aged 30 days compared to SAXS patterns of β-SSS. The arrows evidenced the FAs crystalline phases.

Table 3
d-spacing values of the multiple phases observed in binary mixtures 90SSS/10FAs. The lamellar thickness (D) values of α-SSS and β-SSS are also reported.

Sample	d-spacing (Å)			Crystallite size D of α-SSS (nm)
	α-SSS	β-SSS	d-spacing (Å)	
90SSS/10LA	–	45.0	27.3	–
90SSS/10MA	50.4	45.3	31.6	71.2
90SSS/10PA	50.3	45.1	35.7	74.1
90SSS/10SA	50.0	–	–	103.8

was the only one showing SSS entirely in the stable β polymorph (*d*-spacing = 44.83 Å). In the blends containing FAs with C > 12, SSS was for the majority still in the α form (*d*-spacing of about 50 Å), with only a small fraction transformed in the stable polymorph. This fraction decreased in the order MA > PA > SA, as evident from the third-order reflections, which were deconvoluted to calculate the areas of the two different phases. The results indicated that the percentage values of α-SSS after 30 days from crystallization were 87 %, 92 % and 100 % for MA, PA and SA, respectively. 90SSS/10SA showed only one lamellar phase of *d*-spacing = 50.0 Å corresponding to that of α-SSS without any additional phase attributable to pure SA. Interestingly, the lamellar thickness of this crystalline phase was lower (50.0 Å) compared to the other binary mixtures and to pure α-SSS (50.3 Å). Therefore, we can conclude that, at a 90/10 composition, SA is miscible with α-SSS as they form a solid solution having a single lamellar phase with *d*-spacing slightly lower than that of the pure TAG. Thus, the incorporation of SA in the crystalline structure allowed SSS to organize in a tightly packed crystals and this structure seemed to stabilize the α-polymorph.

In addition to the SSS polymorphs, other lamellar phases were observed in 90SSS/10LA, 90SSS/10MA and 90SSS/10PA systems, highlighted in Fig. 2 with the arrows. In the LA-containing sample, the SAXS pattern showed an intense and sharp first order peak with equal position (27.3 Å) to pure LA, whereas in 90SSS/10MA system, the peaks related to pure MA appeared broader; however, their maximum (31.6 Å) corresponded to the position of the first order SAXS peak of MA polymorph C. In 90SSS/10PA system, only very low intensity first order and third order peaks of pure PA (*d*-spacing 35.7 Å) were detected. The intensity of SAXS peaks related to the FA phase, decreasing in the order LA > MA > PA suggested that the integration of equal amounts of FAs in the crystal lattice of the TAG increased proportionally with the chain similarity with SSS.

The average crystallite size of α-SSS in the blends was also calculated (Table 3). The obtained values remain within the same order of magnitude of that of freshly crystallized pure α-SSS, which exhibits a crystallite size of 91.5 nm (Bertoni et al., 2024). However, a clear difference was observed between the blends containing MA and PA, showing crystallites of about 70–75 nm, and the solid solution system 90SSS/10SA, where the α-SSS crystallites were larger (103.8 nm).

3.2.2. *Microstructure*

The differences observed between the SSS/FA systems in terms of miscibility and polymorphisms suggested that the crystal morphologies of the binary mixtures may be also different, depending on the type of FA. Light microscopy images with polarized filter (Fig. 3) revealed the presence of spherulitic structures that extend radially from a single point, typical of SSS, with shapes ranging from spherical to angular in all samples and size between 30 and 100 μm. Clear differences were observed between the blends with LA and MA and those with PA and SA. In the first cases, the SSS spherulities were surrounded by crystals appearing white under polarized light (blue arrows), which can be attributed to the highly birefringent FAs crystallized as separate phase. Differently, no highly birefringent crystalline phase was observed in the mixtures with longer chain FAs. 90SSS/10PA sample showed a heterogeneous microstructure with small spherulities, while 90SSS/10SA

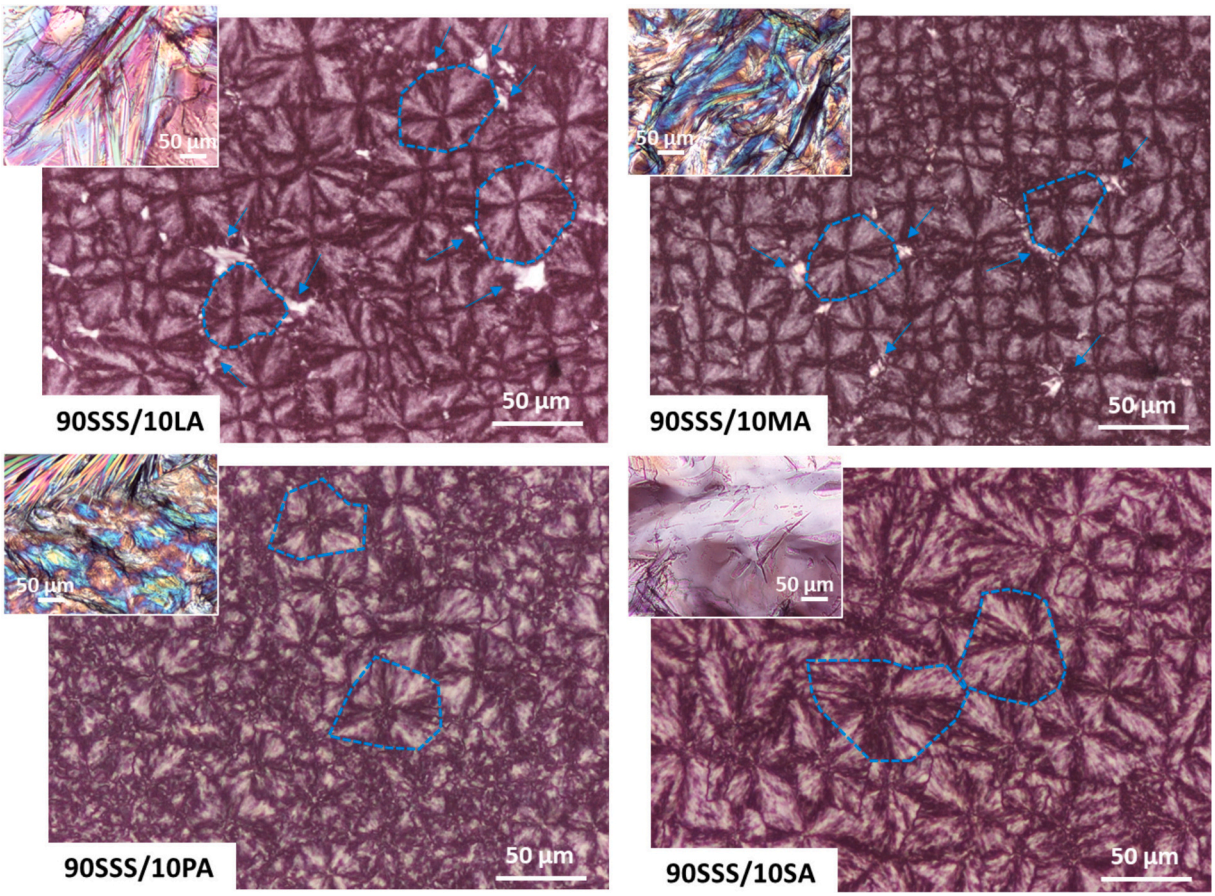

Fig. 3. Polarized light microscopy images of 90SSS/10LA, 90SSS/10MA, 90SSS/10PA and 90SSS/10SA analysed 30 days after crystallization. The spherulities edges are evidenced with blue circles and the second crystalline phase of pure FA ss evidenced by blue arrows. Side insets show the PLM image of the respective pure FAs: LA, MA, PA and SA. (For interpretation of the references to colour in this figure legend, the reader is referred to the web version of this article.)

sample presented a uniform microstructure with well-defined spherulites of variable size. These observations confirmed the miscibility/mixing behaviour of the various SSS/FA systems.

3.2.3. In situ crystallization and polymorphic evolution monitored by synchrotron- SAXS

DSC, SAXS, and PLM studies clearly showed that the effect of free FAs on a model saturated TAG depends on the FA chain length, specifically: (i) The α-polymorph of TAG is miscible with 10 % FAs with equal chain length. The FAs are incorporated into the crystalline structure, enhancing TAG molecular packing and resulting in a single lamellar phase with a slightly reduced *d*-spacing compared to pure α-TAG;

(ii) The miscibility of the TAG with FAs decreases as the difference in chain length increase (e.g. C16 > C14 > C12). The immiscibility can be attributed to the mismatch in fatty acid chain lengths between the FAs and SSS, which increases instability in the terminal methyl regions of the SSS lamellae and hinders the co-accommodation of both molecules within the same lamellar phase, as already noted elsewhere (Macridachis González et al., 2023).

However, it is unclear whether the progressive transformation of SSS from the α- to the β-form is the cause of the exclusion of LA/MA/PA molecules which, being immiscible with the β-form, end up crystallizing as a separate phase or, conversely, if the poor miscibility of FAs with α-SSS leads to the early nucleation of pure LA/MA/PA, with these nuclei then offering a template which decreases activation energy for heterogeneous nucleation of β-crystals. To clarify which of these two hypotheses better describes the systems under investigation, time-resolved measurements were carried out by synchrotron SAXS analysis while performing temperature ramps.

The SAXS data of 90SSS/10LA obtained during real-time crystallization (Fig. 4A) showed that, after SSS crystallization in the kinetically favoured α-form at about 55 °C, the lamellae of pure LA (*d*-spacing = 27.5 Å) crystallized as separate phase during fast cooling at about 37 °C. This was not the case for 90SSS/10SA systems, which showed only the crystallization of a single lamellar phase during cooling (Fig. 4B). Overall, the data indicated that SSS crystallized from the melt in the kinetically favoured α-form and no crystallization in the β phase was observed. The transition of SSS from α to β should be therefore a solid-solid transformation as it starts at about 35 °C (Fig. 4A), below the melting temperature of the involved polymorphs. In case of 90SSS/10LA, it appeared that the early nucleation of LA is the initial event which precedes the α → β transition of SSS.

Thus, a key factor influencing the SSS/FAs behaviour is miscibility, i.e. the ability of two substances to mix at the molecular level and form a homogeneous phase. In lipid systems, miscibility can vary significantly depending on the crystalline form of the components involved. The miscibility of each specific minor component in a TAG blend depends not only on the chemical identity and polymorphic form of the minor component itself, but also on the polymorphic state of the TAG, due to differences in molecular packing and intermolecular interactions. While a single solid solution phase is formed in 90SSS/10SA blend, SSS mixtures with 10 % FAs of chain length C16, C14 and C12 were found to be immiscible with β-SSS and only partially miscible with α-SSS, forming a solid solution with a miscibility limit below 10 % FA content. Interestingly, these partially miscible systems appeared to accelerate the polymorphic transformation of the TAGs to their stable crystalline form.

This aspect was investigated by monitoring the polymorphism of the mixtures by time-resolved SAXS/WAXS measurements at constant

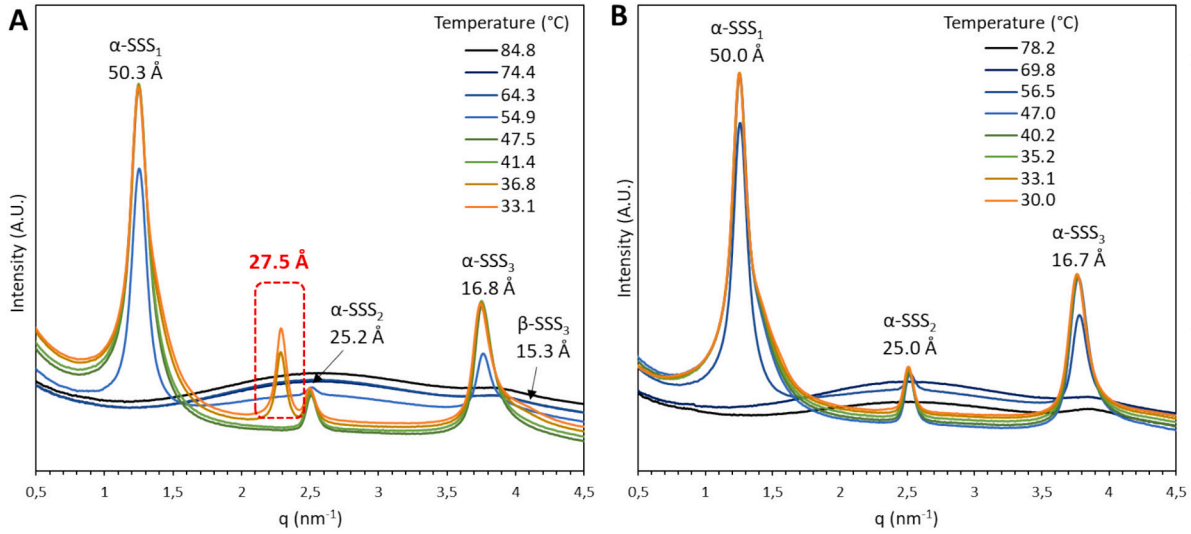

Fig. 4. Time-resolved SAXS data of (**A**) 90SSS/10LA and (**B**) 90SSS/10SA samples obtained during the cooling phase at −10 °C/min from the melt (90 °C). Region of q between 0.5 and 4.5 nm^{-1} is shown.

temperatures. Fig. 5 shows the SAXS spectra collected during the two steps isothermal phase (1 h at 30 °C and 1 h at 40 °C) after crystallization of the samples. To better appreciate the influence of the specific FAs on the polymorphic transformation of SSS, the SAXS data collected during the isothermal step at 40 °C were used for quantitative phase analysis. Specifically, the areas of the first-order peaks corresponding to the α- and β-polymorphs of SSS were used to quantify the relative abundance of the coexisting phases observed in the time-resolved SAXS scans and

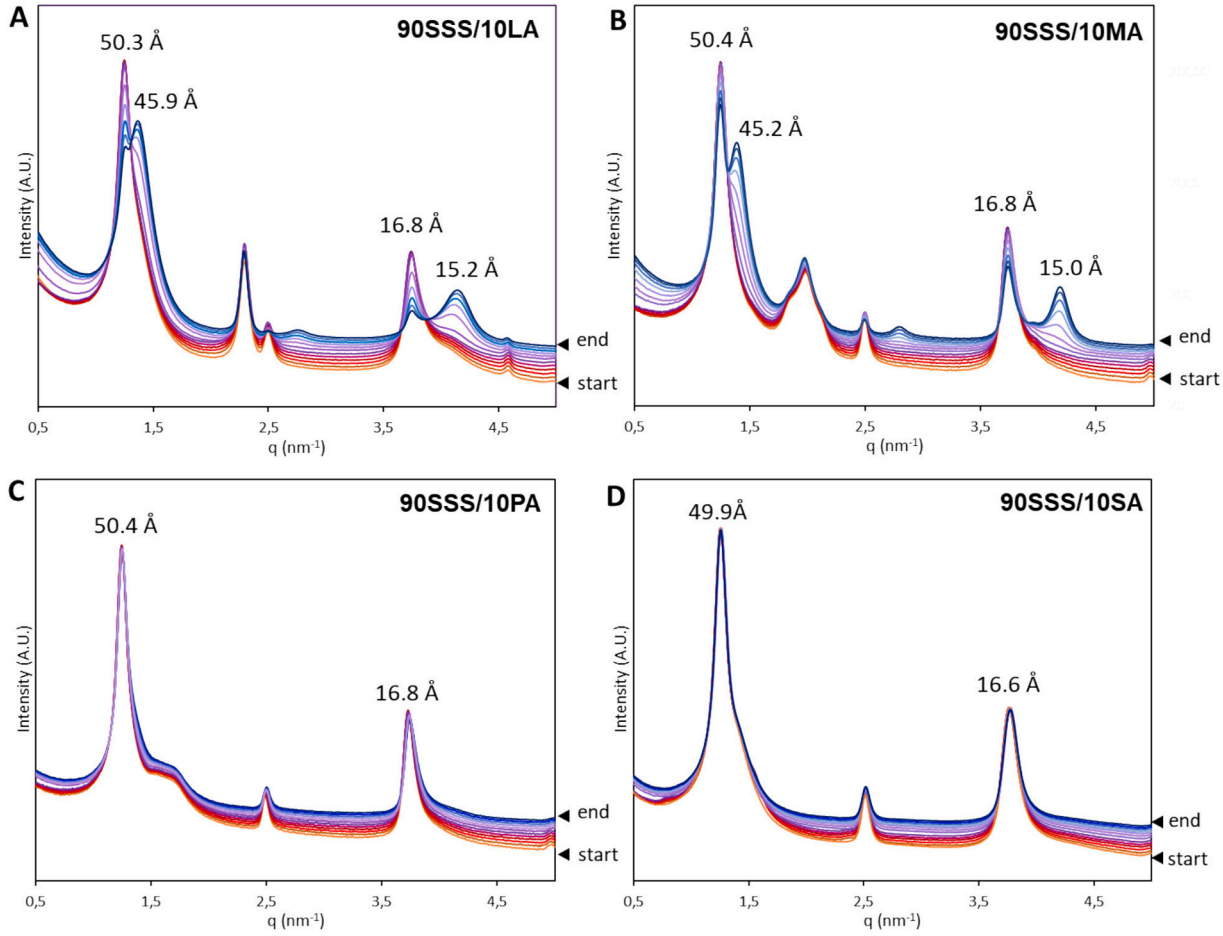

Fig. 5. Time-resolved SAXS data of SSS/FAs samples obtained at various time points during the isothermal phase (1 h at 30 °C followed by 1 additional hour at 40 °C) when cooled at −10 °C/min from the melt (90 °C). The figure shows the SAXS pattern of (**A**) 90SSS/10LA, (**B**) 90SSS/10MA, (**C**) 90SSS/10PA and (**D**) 90SSS/10SA in the q region between 0.5 and 5 nm^{-1}.

the resulting kinetic curves are presented in Fig. 6.

Fig. 5 and Fig. 6 showed that the extent of the SSS polymorphic transformation differed among the four samples and tended to decrease with increasing fatty acid chain length, following the general trend LA > MA > PA > SA. Specifically, the kinetic curves (Fig. 6) allowed a quantitative comparison on the effect of the various FAs on the polymorphic transition rate of SSS. The kinetic profile for the 90SSS/10LA system showed a steep curve, indicating a rapid transformation rate and after 60 min at 40 °C the percentage of β-SSS was 84.2 %. However, the newly formed β-SSS phase observed in the mixture had larger lamellar thickness (45.9 Å) compared to pure β-SSS (44.8 Å, Fig. 1SI), suggesting that the rapid polymorphic conversion correlates with the formation of imperfect crystals with a less packed structure. Conversely, the system 90SSS/10MA allowed, in the same conditions, the transformation of 44.1 % of SSS into a tighter packed β-phase (*d*-spacing of 45.2 Å). Differently, in the system 90SSS/10PA only a small shoulder could be observed in the first order peak (Fig. 5C); whereas for the 90SSS/10SA sample, the peaks related to the β-lamellar phase were almost undetectable and only the peaks of α-SSS were visible (Fig. 5D). The relative kinetic curves confirmed the very slow α → β transition with only 4.4 % and 2.2 % of β-SSS formed in the samples containing PA and SA, respectively.

Thus, these data evidenced the role of shorter chain FAs, specifically LA, in improving the α → β transition of SSS. To investigate the underlying mechanism of this phenomenon, we focused on the SSS/LA binary system, which demonstrated the most pronounced α → β transformation of SSS.

3.3. SSS/LA blends

3.3.1. Phase behaviour and miscibility limit

To better investigate this system, α-SSS/LA blends covering the entire set of compositions were crystallized and analysed by DSC (Fig. 7A). DSC measurements showed one or two peaks for each of the SSS/LA binary mixtures, indicating an immiscible system with eutectic behaviour. The relative phase diagram (Fig. 7B) and the Tammann plot (Fig. 7C) confirmed the eutectic composition at approximately 20 % mass percentage of LA. At this ratio, both components melted simultaneously as the DSC showed only one melting peak with $T_{onset} = 41.5$ °C and $\Delta H = 39.75$ J/g.

In the phase diagram, the endothermic events related to the melting of α-SSS and that of the stable β-SSS formed during the heating scan are shown. The exothermic transformation of α → β is not included, since its position and intensity appeared to be highly variable. Regarding the eutectic composition, a linear regression analysis was performed on the two segments of the Tammann plot before and after the eutectic point. The eutectic composition, determined from the intersection of the regression lines, was found to be a mixture containing 20.36 wt% LA. Analogous eutectic behaviour was found for α-SSS/MA system (Fig. 4SI) but the eutectic composition presented higher amount of MA (around 30–40 %). The Tammann plot also allows estimation of the miscibility limit (solvus), which corresponds to the composition at which the eutectic endotherm reaches zero (left grey line). Specifically, the calculated solvus composition, based on the point at which the enthalpy becomes zero, is 3.5 % LA. In addition, a solid solution also appears to form on the right side of the plot, where LA is the majority component, with the calculated solvus composition at 88.3 % LA.It should be noted that the phase diagram reported for the α-SSS/LA system does not represent a true equilibrium phase diagram, since α-SSS is a metastable polymorph recrystallized from the melt. Nevertheless, this diagram, kinetic rather than thermodynamic in nature, provide valuable insights into the behaviour of the SSS/LA blends under given experimental conditions.

DSC analyses were performed also on mixtures of β-SSS and LA at different compositions. As shown by the DSC curves (Fig. 8A) and the relative phase diagram (Fig. 8B), also β-SSS is immiscible with LA in the solid state, but, differently from α-SSS, their phase behaviour is monotectic rather than eutectic. In systems with monotectic behaviour, solidification produces a mixture of crystals of the components without the simultaneous melting depression of both phases. Unlike eutectic systems, where both components show melting point depression, in monotectic systems only the high melting component (in our case, β-SSS) exhibits melting point depression.

The insights gained from the phase diagrams clarified the nature of the low-melting DSC peak in freshly crystallized samples containing 10 % of LA and 10 % of MA evidenced in Fig. 1. The eutectic peak is observed in freshly crystallized samples, but its intensity decreased with the aging time and ultimately disappeared once all SSS converted to the β-form. This behaviour can be explained considering the progressive depletion of α-SSS due to the α → β polymorphic conversion.

To complement these results, the miscibility limit of LA in α-SSS was investigated by SAXS/WAXS analysis. SSS/LA mixtures with LA content equal to 2.5 %, 5 % and 10 % were crystallized, aged for 1 or 30 days at 25 °C, and analysed by SAXS coupled with WAXS. In contrast to SAXS, which provides information on the lamellar repeat distance, WAXS reflections arise from the lateral packing of the acyl chains and allow the identification of the different TAG polymorphs. The SAXS and WAXS patterns of these samples (Fig. 9) showed the coexistence of three crystalline phases: α-SSS, β-SSS and LA polymorph C.

The results clearly indicated that the proportion of β-SSS relative to α-SSS increased with the amount of LA (Fig. 9). For instance, in the sample containing 10 % LA, the majority of SSS had already transformed

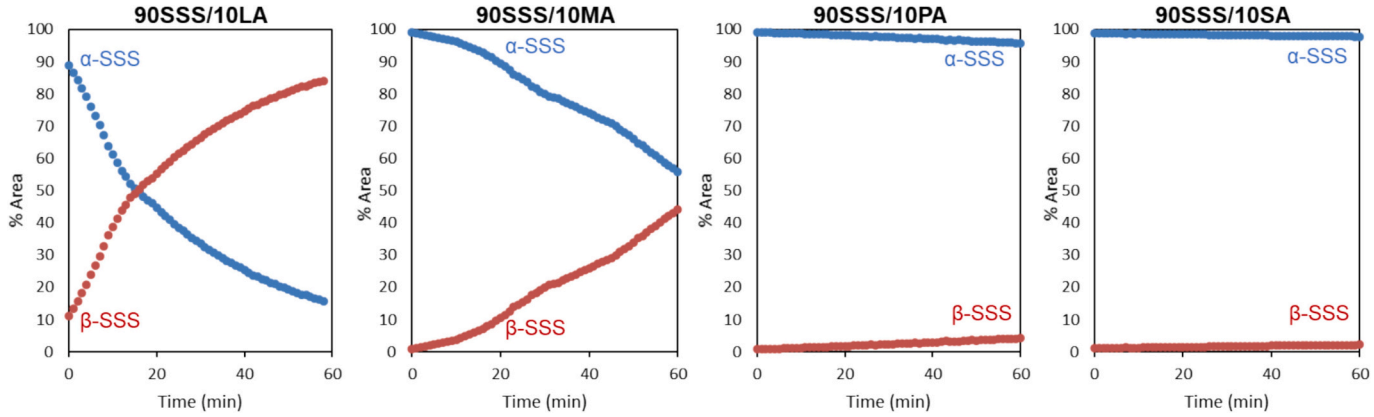

Fig. 6. SSS α → β transition kinetic in the SSS/FAs samples during the 1 h isothermal phase at 40 °C. The blue dots represent the relative area % of the α-SSS phase; the red dots represent the relative area % of the β-SSS phase. (For interpretation of the references to colour in this figure legend, the reader is referred to the web version of this article.)

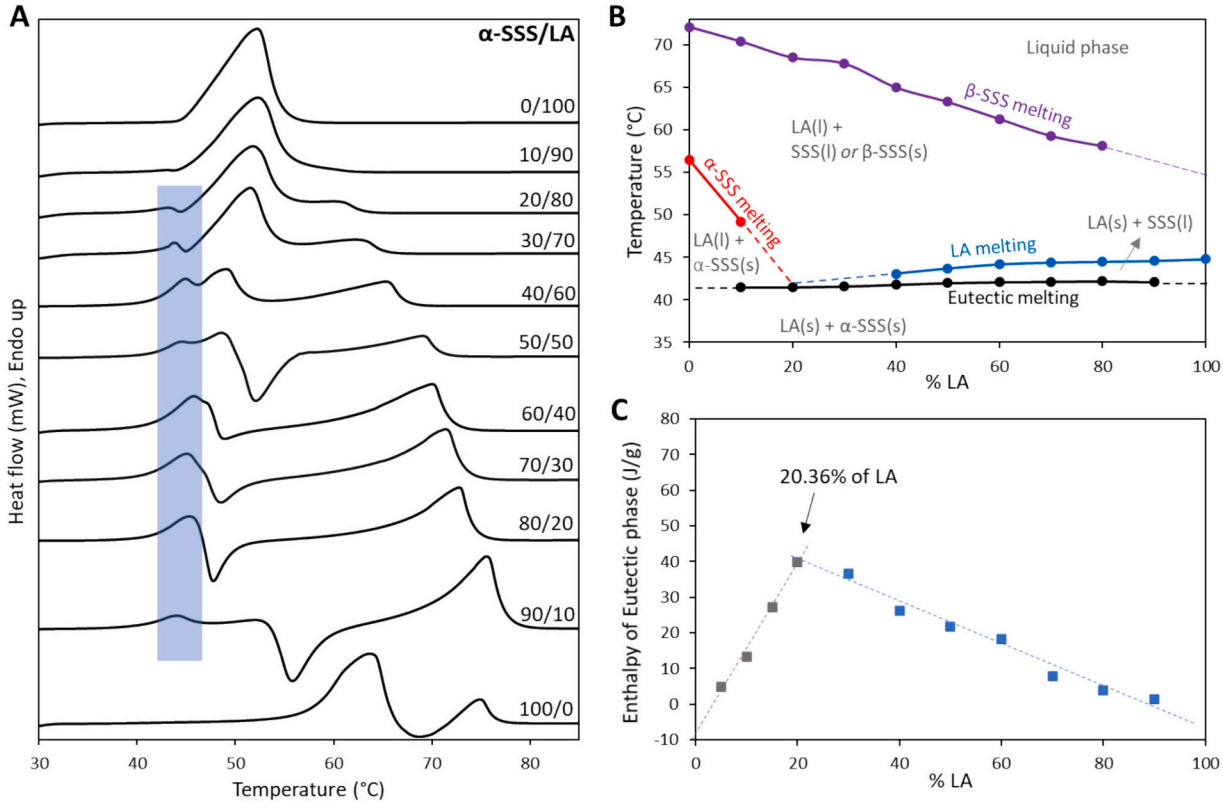

Fig. 7. DSC melting curves of α-SSS/LA binary mixtures at the different mass proportion (**A**), relative phase diagram (**B**) and Tammann plot (**C**).

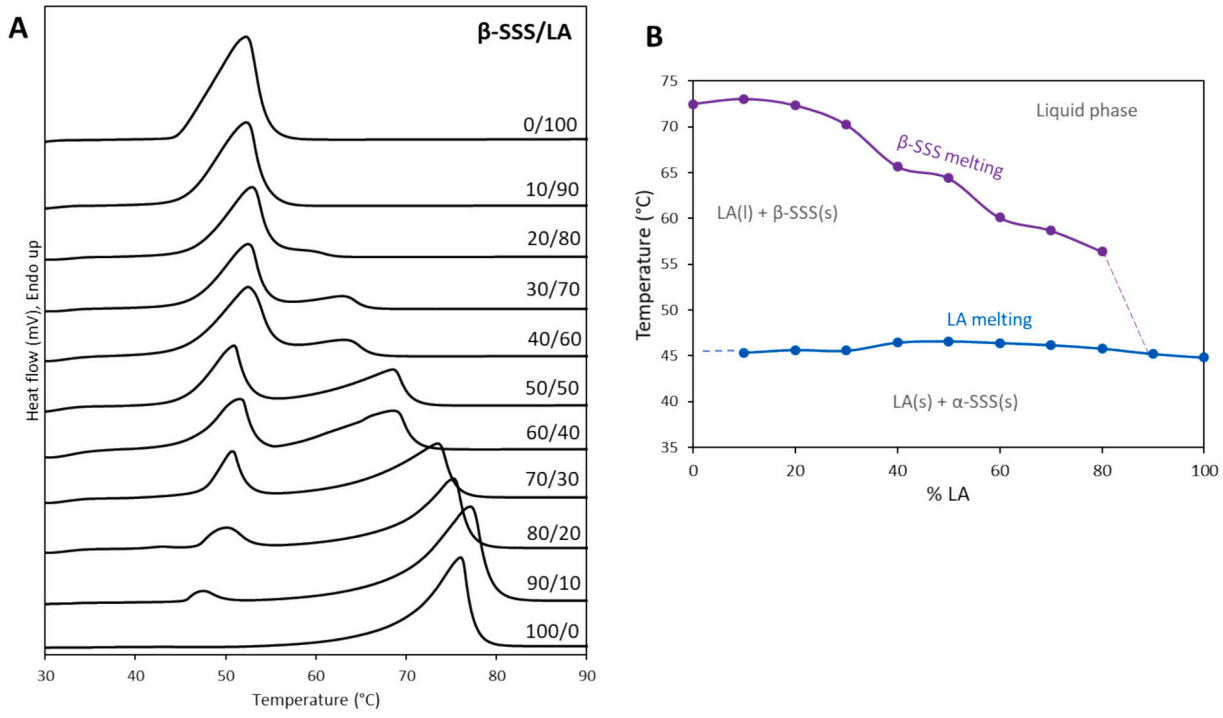

Fig. 8. DSC melting curves of β-SSS/LA binary mixtures at the different mass proportion (**A**) and relative phase diagram (**B**).

into the stable β-form after just one day (Fig. 8A). In contrast, blends with lower LA content showed a slower α → β transformation. Notably, with 2.5 % LA, the lamellar phase of α-SSS was still detectable even after 30 days (Fig. 8B). Samples with 10 % and 5 % LA displayed an additional lamellar phase corresponding to polymorph C of LA, as evidenced by a distinct SAXS peak (red arrows) at $q = 2.3\ nm^{-1}$, while it was absent in the 97.5SSS/2.5LA mixture. Since the limit of detection of synchrotron SAXS for multiphase systems is well below 1 %, typically in the range 0.005 %–0.4 % in case of solid samples (Munjal & Suryanarayanan, 2021), the absence of the LA signal in the mixture 97.5SSS/2.5LA can be

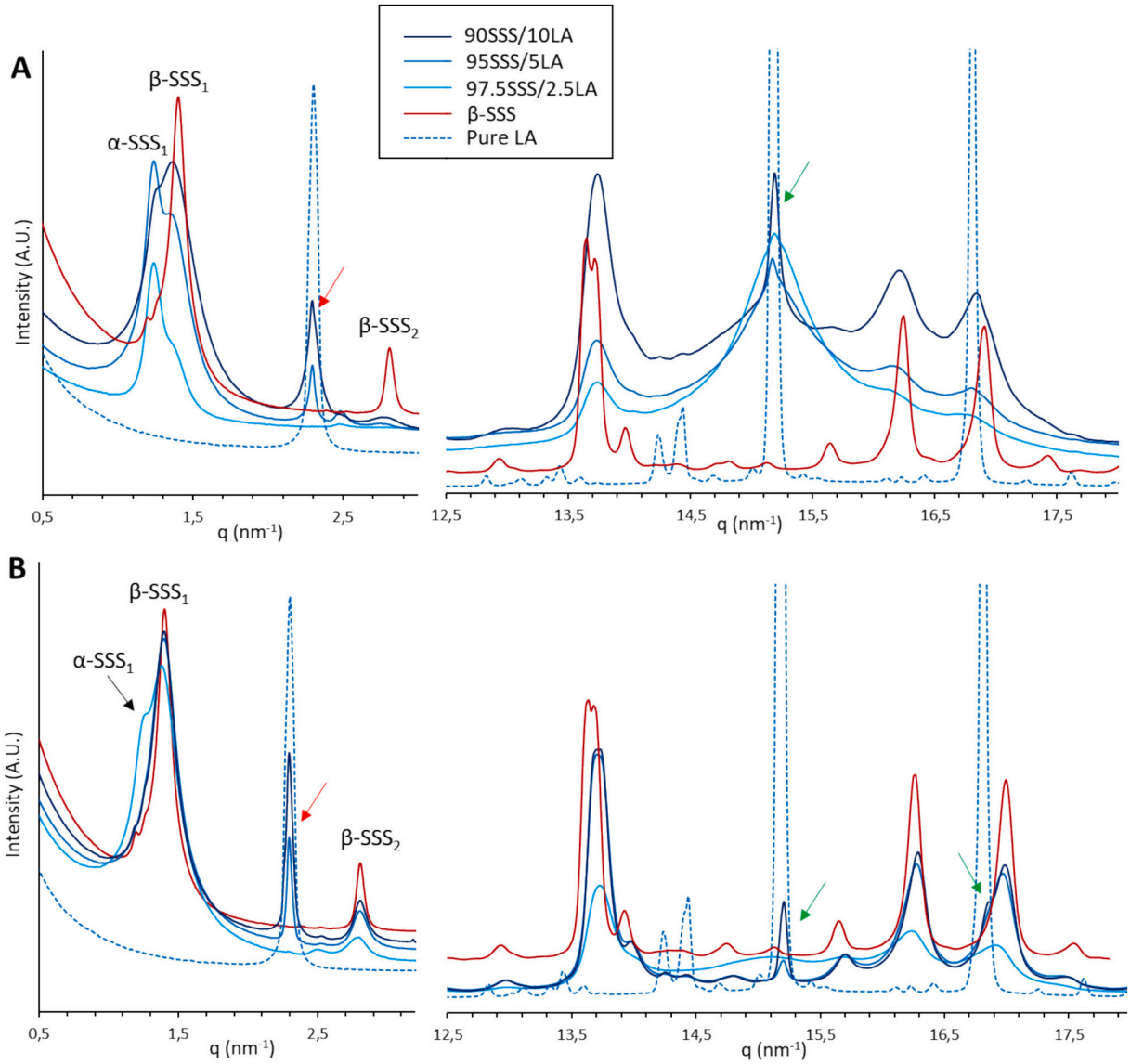

Fig. 9. SAXS and WAXS patterns of 90SSS/10LA, 95SSS/5LA and 97.5SSS/2.5LA systems aged for 1 day (**A**) and 30 days (**B**) collected at 25 °C, compared to SAXS and WAXS patterns of pure LA and β-SSS. Peaks related to LA phase in the mixtures are marked by red and green arrows. (For interpretation of the references to colour in this figure legend, the reader is referred to the web version of this article.)

considered a reliable data to estimate the solvus composition. Therefore, the miscibility limit of LA in α-SSS must be between 5 and 2.5 %, which is consistent with the solvus composition of 3.5 % LA calculated from the Tammann plot (Fig. 7C).

The *d*-spacing values and the calculated crystallite thicknesses for the α-SSS phase in the SSS/LA blends are reported in Table 4. The average crystallite size of α-SSS decreased progressively with increasing LA content, from 85.8 to 73.6 to 69.8 nm. Consistently with what observed for SSS/MA and SSS/PA blends (Table 3), these values are lower than that of pure α-SSS, equal to 91.5 nm (Bertoni et al., 2024). A decrease in D was observed also with the aging time, as the crystallite thickness of the 97.5SSS/2.5 LA blend passed from 85.8 nm to 55.3 nm after 30 days. This trend was previously observed also in pure SSS without additives (Bertoni et al., 2024) and can be attributed to the progressive α-to-β polymorphic conversion.

Additionally, the *d*-spacing values and the crystallite thicknesses for

Table 4
d-spacing values and crystallite thicknesses for the α-SSS phase in 90SSS/10LA, 95SSS/5LA and 97.5SSS/2.5LA systems aged for 1 and 30 days.

Sample	Day 1		Day 30	
	d-spacing (Å)	Crystallite size D (nm)	d-spacing (Å)	Crystallite size D (nm)
97.5SSS/2.5 LA	50.78	85.8	50.00	55.3
95SSS/5LA	50.38	73.6	–	–
90SSS/10LA	50.37	69.8	–	–

Table 5
d-spacing values and crystallite thicknesses for the LA phase in 90SSS/10LA, 95SSS/5LA and 98.5SSS/2.5LA systems aged for 1 and 30 days.

Sample	Day 1		Day 30	
	d-spacing (Å)	Crystallite size D (nm)	d-spacing (Å)	Crystallite size D (nm)
98.5SSS/2.5 LA	–	–	–	–
95SSS/5LA	27.40	158.2	27.35	198.3
90SSS/10LA	27.38	128.5	27.35	190.0

the LA phases in the blends were determined and are shown in Table 5. Interestingly, although the *d*-spacing did not change significantly, the crystallite thickness increased with the aging time. This growth can be interpreted as a spontaneous ripening process of the LA phase over time, occurring concurrently with the transformation of SSS from the α to the β polymorph. The pressure exerted by the enlarging LA crystals may facilitate the diffusion of SSS molecules toward the β-phase crystals.

The nature of the LA phase and its miscibility limit were confirmed by WAXS data (green arrows in Fig. 8): although of low intensity, the peak positions indicated that LA crystallized in its original crystal form (polymorph C). In particular, the main peak at $q = 15.2\ nm^{-1}$, corresponding to the primary reflection at 21.6° 2θ, characteristic of the polymorph C of LA (see Fig. 2SI), was observed in the blends containing 5 % and 10 % LA, but not in that containing 2.5 % LA.

Finally, the effect of low LA amounts, either below (2.5 %) or above (5 %) its solubility limit, on SSS polymorphic transition was investigated by real-time SAXS measurements and the kinetics of the α → β transition at 40 °C are shown in Fig. 10. The data clearly showed that decreasing LA amount led to slower SSS polymorphic transition.

Thus, the enhanced α → β transition of SSS observed in the blends with LA can be explained by the interplay of microstructural, molecular, and thermodynamic factors.

One factor is the smaller crystallite size of α-SSS in the eutectic mixture (Table 3) compared to those of pure α-SSS or α-SSS solid solution (as the case of 90SSS/10SA, Table 2). Generally, eutectic mixtures are characterized by a fine microstructure consisting of alternating crystallites of the two constituent phases. The significant reduction in the individual solid phases led to enhanced surface area and altered physicochemical properties (i.e. the melting point) (Bazzo et al., 2020). It has been demonstrated that the kinetic of phase transitions observed in TAGs are influenced by the material size. Specifically, while the type of transition (e.g. α → β' → β) remains unchanged, systems of smaller size (e.g. colloidal nanoparticles) showed significant increase in terms of rate of polymorphic transitions compared to bulk lipids (Higami et al., 2003). At the molecular level, the presence of lattice defects, such as dislocations or stacking faults, caused by the incorporation of LA crystals into the SSS crystalline network, which have been shown to trigger polymorphic transitions (Cholakova & Denkov, 2024). Finally, incorporation of minor amounts of FA into the SSS lattice can alter the relative free energy of the polymorphs, changing the thermodynamic driving force for the α → β transition. However, this thermodynamic effect alone cannot explain the observed kinetics: if it were the only factor, blends with LA in excess of the solvus (5–10 % LA) would be expected to convert at similar rates, since the solid solution phase composition is the same. Instead, our data show that eutectic behaviour with excess LA outside the solvus influences the rate of conversion, suggesting that a combination of mechanisms act together to accelerate the α → β transition.

Overall, these data demonstrated that the higher the amount of immiscible LA phase in the mixture, the fastest the TAG α → β polymorphic transition. This effect is similar to that of liquid additives, which speed up the transformation of tristearin into the β-form at 5–10 % *w*/w (Bertoni et al., 2021, 2024). While in the latter case the accelerated transition was attributed to enhanced molecular mobility provided by the liquid phase, in case of solid additives such as LA, it is more likely driven by a combination of thermodynamic factor with structural changes, such as the FAs smaller domain size of SSS, increased surface area, and structural imperfections caused by the incorporation of LA.

4. Conclusion

The effect of saturated fatty acids (FAs) with chain lengths from C12 to C18 addition on the crystallization behaviour of tristearin (SSS) was investigated. SAXS, PLM, and DSC analyses revealed that the miscibility between SSS and FAs decreases with increasing chain length mismatch (C18 > C16 > C14 > C12). In particular, due to the four-carbon difference in chain length, the α-SSS/LA system exhibits eutectic behaviour, with eutectic point at 20 wt% LA and low miscibility limit (between 2.5 wt% and 5 wt% LA). Time-resolved SAXS measurements allowed to compare the impact of different FAs on the α → β polymorphic transition of SSS. It was found that the conversion rate of α-SSS to the stable β form increases with the amount of immiscible LA phase. Specifically, this effect is attributed to the smaller size of α-SSS crystallites, which leads to a higher surface area of the α-SSS phase, potentially facilitating rearrangement into the β-form. In addition, the presence of LA crystallites embedded within the crystalline network may introduce lattice imperfections and local strain, both of which can increase the rate of polymorphic transition. These findings provide valuable insights into the role of FAs as minor component in TAG-based edible systems and highlight the interplay between fat miscibility, nano/microstructure and polymorphic transitions. It would be interesting to investigate whether this effect extend to TAGs with different chain lengths or more complex fat mixtures, in order to better understand their implications for lipid-based foods and ultimately enable improved control over crystallization behaviour, long-term stability, and functional properties of these products.

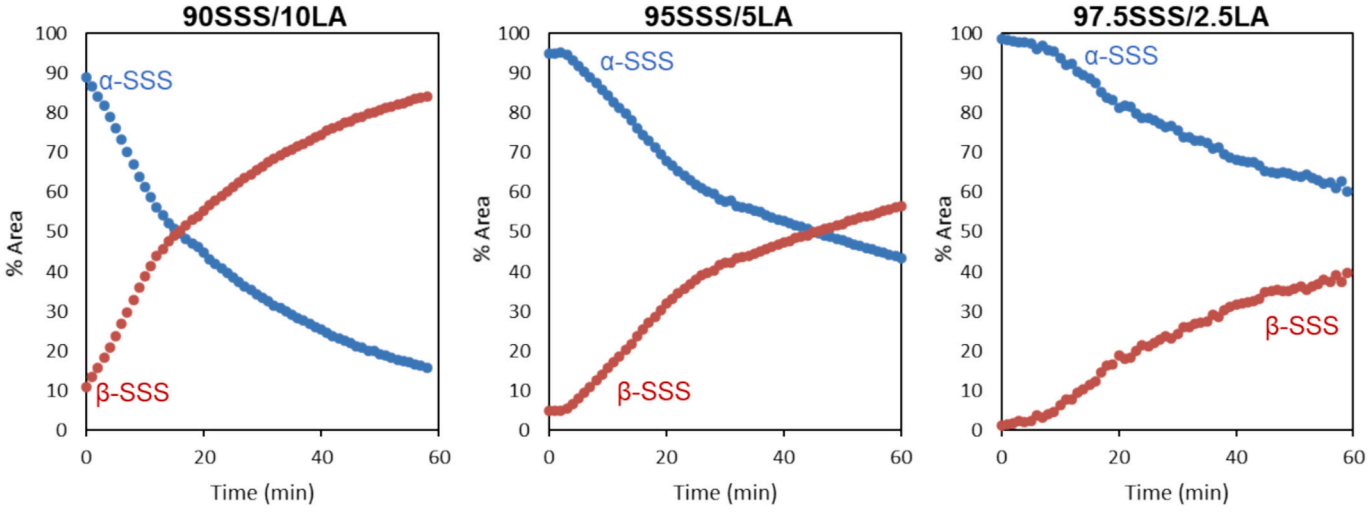

Fig. 10. SSS α → β transition kinetic in the SSS/LA samples with varying LA amount during the 1 h isothermal phase at 40 °C. The blue dots represent the relative area % of the α-SSS phase; the red dots represent the relative area % of the β-SSS phase. (For interpretation of the references to colour in this figure legend, the reader is referred to the web version of this article.)

CRediT authorship contribution statement

Serena Bertoni: Writing – review & editing, Writing – original draft, Investigation, Conceptualization. **Elena Simone:** Writing – review & editing, Investigation. **Beatrice Albertini:** Writing – review & editing. **Nadia Passerini:** Writing – review & editing, Funding acquisition.

Declaration of competing interest

The authors declare the following financial interests/personal relationships which may be considered as potential competing interests: Elena Simone reports financial support was provided by European Research Council (ERC). If there are other authors, they declare that they have no known competing financial interests or personal relationships that could have appeared to influence the work reported in this paper.

Acknowledgments

We acknowledge CERIC for funding for beamtime on the Austrian SAXS beamline at Elettra Sincrotron Trieste (Italy) under proposals 20222033, 20227148 and 20242069 (CERIC). We are grateful to beamline scientists Dr. Barbara Sartori, Dr. Benedetta Marmiroli, and Dr. Sigrid Bernstorff for the help and support with the setup used for the work. Elena Simone has received funding from the European Research Council (ERC) under the European Union's Horizon 2020 research and innovation programme (grant agreement No. 949229, CryForm).

Appendix A. Supplementary data

Supplementary data to this article can be found online at https://doi.org/10.1016/j.foodres.2025.117766.

Data availability

Data will be made available on request.

References

Acevedo, N. C., Block, J. M., & Marangoni, A. G. (2012). Unsaturated emulsifier-mediated modification of the mechanical strength and oil binding capacity of a model edible fat crystallized under shear. *Langmuir, 28*(46), 16207–16217. https://doi.org/10.1021/la303365d

Albertini, B., Passerini, N., Pattarino, F., & Rodriguez, L. (2008). New spray congealing atomizer for the microencapsulation of highly concentrated solid and liquid substances. *European Journal of Pharmaceutics and Biopharmaceutics, 69*(1), 348–357. https://doi.org/10.1016/j.ejpb.2007.09.011

Bazzo, G. C., Pezzini, B. R., & Stulzer, H. K. (2020). Eutectic mixtures as an approach to enhance solubility, dissolution rate and oral bioavailability of poorly water-soluble drugs. *International Journal of Pharmaceutics, 588*, Article 119741. https://doi.org/10.1016/j.ijpharm.2020.119741

Bertoni, S., Dolci, L. S., Albertini, B., & Passerini, N. (2018). Spray congealing: A versatile technology for advanced drug-delivery systems. *Therapeutic Delivery, 9*(11), 833–845. https://doi.org/10.4155/tde-2018-0049

Bertoni, S., Passerini, N., & Albertini, B. (2021). Liquid lipids act as polymorphic modifiers of tristearin-based formulations produced by melting technologies. *Pharmaceutics, 13*(7). https://doi.org/10.3390/pharmaceutics13071089

Bertoni, S., Simone, E., Sangiorgi, S., Albertini, B., & Passerini, N. (2024). The use of polymorphic state modifiers in solid lipid microparticles: The role of structural modifications on drug release performance. *European Journal of Pharmaceutical Sciences, 192*, Article 106650. https://doi.org/10.1016/j.ejps.2023.106650

Chaleepa, K., Szepes, A., & Ulrich, J. (2010). Effect of additives on isothermal crystallization kinetics and physical characteristics of coconut oil. *Chemistry and Physics of Lipids, 163*(4), 390–396. https://doi.org/10.1016/j.chemphyslip.2010.03.005

Cholakova, D., & Denkov, N. (2024). Polymorphic phase transitions in triglycerides and their mixtures studied by SAXS/WAXS techniques: In bulk and in emulsions. *Advances in Colloid and Interface Science, 323*, Article 103071. https://doi.org/10.1016/j.cis.2023.103071

Da Silva, R. C., De Martini Soares, F. A. S., Maruyama, J. M., Dagostinho, N. R., Silva, Y. A., Ract, J. N. R., & Gioielli, L. A. (2016). Microscopic approach of the crystallization of tripalmitin and tristearin by microscopy. *Chemistry and Physics of Lipids, 198*, 1–9. https://doi.org/10.1016/j.chemphyslip.2016.04.004

Denke, M., & Grundy, S. (1991). Effects of fats high in stearic acid on lipid and lipoprotein concentrations in men. *The American Journal of Clinical Nutrition, 54*(6), 1036–1040. https://doi.org/10.1093/ajcn/54.6.1036

Dos Santos Carvalho, J. D., Oriani, V. B., de Oliveira, G. M., & Hubinger, M. D. (2021). Solid lipid microparticles loaded with ascorbic acid: Release kinetic profile during thermal stability. *Journal of Food Processing and Preservation, 45*(6), Article e15557. https://doi.org/10.1111/jfpp.15557

Garti, N., Schlichter, J., & Sarig, S. (1986). Effect of food emulsifiers on polymorphic transitions of cocoa butter. *Journal of the American Oil Chemists' Society, 63*(2), 230–236. https://doi.org/10.1007/BF02546144

Gordon, M. H., & Rahman, I. A. (1991). Effects of minor components on the crystallization of coconut oil. *Journal of the American Oil Chemists Society, 68*(8), 577–579. https://doi.org/10.1007/BF02660154

Gunstone, F. D. (2004). *The chemistry of oils and fats: Sources, composition, properties, and uses*. Blackwell Pub.

Hernández-Veloz, M. J., Rousseau, D., Dibildox-Alvarado, E., Pérez-Meza, L. V., Reyes-Hernández, J., Ruiz-Cabrera, M. A., & Pérez-Martínez, J. D. (2023). Phase diagrams and microstructure of mixtures of n-hentriacontane and saturated fatty acids. *Thermochimica Acta, 728*, Article 179595. https://doi.org/10.1016/j.tca.2023.179595

Higami, M., Ueno, S., Segawa, T., Iwanami, K., & Sato, K. (2003). Simultaneous synchrotron radiation X-ray diffraction-DSC analysis of melting and crystallization behavior of trilauroylglycerol in nanoparticles of oil-in-water emulsion. *Journal of the American Oil Chemists' Society, 80*(8), 731–739. https://doi.org/10.1007/s11746-003-0765-2

Liu, L., Li, L., He, N., Li, B., & Zhang, X. (2022). Effect of emulsifiers on the quality of palm oil based shortening during variable temperature storage. *Journal of Oleo Science, 71*(12), 1735–1741. https://doi.org/10.5650/jos.ess22149

Liu, L., Li, L., Wan, L., Mao, L., Li, B., & Zhang, X. (2021). Addition of glyceryl monostearate affects the crystallization behavior and polymorphism of palm stearin. *Bioprocess and Biosystems Engineering, 44*(5), 941–949. https://doi.org/10.1007/s00449-019-02251-1

Loisel, C., Lecq, G., Keller, G., & Ollivon, M. (1998). Dynamic crystallization of dark chocolate as affected by temperature and lipid additives. *Journal of Food Science, 63*(1), 73–79. https://doi.org/10.1111/j.1365-2621.1998.tb15679.x

Macridachis González, J., Bayés-García, L., & Calvet, T. (2023). Mixing phase behavior of trilaurin and monounsaturated triacylglycerols based on palmitic and oleic fatty acids. *Journal of Thermal Analysis and Calorimetry, 148*. https://doi.org/10.1007/s10973-023-12421-9

Macridachis-González, J., Bayés-García, L., & Calvet, T. (2020). An insight into the solid-state miscibility of triacylglycerol crystals. *Molecules, 25*(19). https://doi.org/10.3390/molecules25194562

Metin, S., & Hartel, R. W. (2005). Crystallization of fats and oils. *In Bailey's Industrial Oil and Fat Products.*. https://doi.org/10.1002/047167849X.bio021

Moreno, E., Cordobilla, R., Calvet, T., Cuevas-Diarte, M. A., Gbabode, G., Negrier, P., … Oonk, H. A. J. (2007). Polymorphism of even saturated carboxylic acids from n-decanoic to n-eicosanoic acid. *New Journal of Chemistry, 31*(6), 947–957. https://doi.org/10.1039/B700551B

Munjal, B., & Suryanarayanan, R. (2021). Applications of synchrotron powder X-ray diffractometry in drug substance and drug product characterization. *TrAC Trends in Analytical Chemistry, 136*, Article 116181. https://doi.org/10.1016/j.trac.2021.116181

Oh, J.-H., McCurdy, A. R., Clark, S., & Swanson, B. G. (2005). Stabilizing polymorphic transitions of tristearin using diacylglycerols and sucrose polyesters. *Journal of the American Oil Chemists' Society, 82*(1), 13–19. https://doi.org/10.1007/s11746-005-1036-y

Pluntze, A. M., Cape, J. L., Klaus, N. D., & Lyon, D. K. (2023). Control of API release with matrix polymorphism in tristearin microspheres. *International Journal of Pharmaceutics, 636*, Article 122806. https://doi.org/10.1016/j.ijpharm.2023.122806

Puppo, M., Martini, S., Hartel, R. W., & Herrera, M. (2006). Effect of sucrose esters on isothermal crystallization and rheological Behaviors of blends of high-melting Milk fat fraction and sunflower oil. *Journal of Food Science, 67*, 3419–3426. https://doi.org/10.1111/j.1365-2621.2002.tb09600.x

Ribeiro, A. P. B., Masuchi, M. H., Miyasaki, E. K., Domingues, M. A. F., Stroppa, V. L. Z., de Oliveira, G. M., & Kieckbusch, T. G. (2015). Crystallization modifiers in lipid systems. Journal of Food Science and Technology, 52(7), 3925–3946. PubMed. doi: https://doi.org/10.1007/s13197-014-1587-0.

Sato, K. (2018). Crystallization of lipids: Fundamentals and applications in food, cosmetics and pharmaceuticals. *Crystallization of lipids: Fundamentals and applications in food, cosmetics and pharmaceuticals*, 508. https://doi.org/10.1002/9781118593882

Seilert, J., Rudolph-Flöter, S., & Flöter, E. (2021). On the relation of entropy and enthalpy of fusion in triglycerides. *European Journal of Lipid Science and Technology, 123*(12), Article 2100098. https://doi.org/10.1002/ejlt.202100098

Silva, R. C., Soares, F. A. S. D. M., Maruyama, J. M., Dagostinho, N. R., Silva, Y. A., Calligaris, G. A., … Gioielli, L. A. (2014). Effect of diacylglycerol addition on crystallization properties of pure triacylglycerols. *Food Research International, 55*, 436–444. https://doi.org/10.1016/j.foodres.2013.11.037

Simone, E., Rappolt, M., Ewens, H., Rutherford, T., Marty Terrade, S., Giuffrida, F., & Marmet, C. (2024). A synchrotron X-ray scattering study of the crystallization behavior of mixtures of confectionary triacylglycerides: Effect of chemical composition and shear on polymorphism and kinetics. *Food Research International, 177*, Article 113864. https://doi.org/10.1016/j.foodres.2023.113864

Smith, K. W., Bhaggan, K., Talbot, G., & van Malssen, K. F. (2011). Crystallization of fats: Influence of minor components and additives. *Journal of the American Oil Chemists' Society, 88*(8), 1085–1101. https://doi.org/10.1007/s11746-011-1819-7

Smith, P. R. (2000). The effects of phospholipids on crystallisation and crystal habit in triglycerides. *European Journal of Lipid Science and Technology, 102*(2), 122–127. https://doi.org/10.1002/(SICI)1438-9312(200002)102:2<122::AID-EJLT122>3.0.CO;2-4

Smith, P. R., Cebula, D. J., & Povey, M. J. W. (1994). The effect of lauric-based molecules on trilaurin crystallization. *Journal of the American Oil Chemists' Society, 71*(12), 1367–1372. https://doi.org/10.1007/BF02541357

Tangsanthatkun, J., & Sonwai, S. (2019). Crystallisation of palm olein under the influence of sucrose esters. *International Journal of Food Science and Technology, 54*(11), 3032–3041. https://doi.org/10.1111/ijfs.14216

Tietz, R. A., & Hartel, R. W. (2000). Effects of minor lipids on crystallization of milk fat-cocoa butter blends and bloom formation in chocolate. *Journal of the American Oil Chemists' Society, 77*(7), 763–771. https://doi.org/10.1007/s11746-000-0122-5

Van Langevelde, A., Peschar, R., & Schenk, H. (2001). Structure of β-trimyristin and β-tristearin from high-resolution X-ray powder diffraction data. *Acta Crystallographica Section B, 57*(3), 372–377. https://doi.org/10.1107/S0108768100019121

Yang, D., Lee, Y.-Y., Lu, Y., Wang, Y., & Zhang, Z. (2024). Internal factors affecting the crystallization of the lipid system: Triacylglycerol structure, composition, and minor components. *Molecules, 29*(8). https://doi.org/10.3390/molecules29081847

Ye, X., Jin, J., Liang, C., Wang, J., Jiang, L., & Zhao, L. (2023). Effects of individual phospholipids on chocolate model systems: Particulate interaction, crystallization behavior, and fat bloom during storage. *Journal of Food Engineering, 357*, Article 111618. https://doi.org/10.1016/j.jfoodeng.2023.111618